International Journal of Materials Science and Applications
2014; 3(2): 58-69
Published online March 30, 2014 (http://www.sciencepublishinggroup.com/j/ijmsa)
doi: 10.11648/j.ijmsa.20140302.18

From transient to permanent phenomena during GMAW of a thin-walled marine aluminium alloy

Stavros K. Chionopoulos*, Dimitris I. Pantelis

Department of Marine Structures, School of Naval Architecture and Marine Engineering, National Technical University of Athens, Greece

Email address:
schionop@gmail.com (S. K. Chionopoulos), pantelis@central.ntua.gr (D. I. Pantelis)

To cite this article:
Stavros K. Chionopoulos, Dimitris I. Pantelis. From Transient to Permanent Phenomena during GMAW of a Thin-Walled Marine Aluminium Alloy. *International Journal of Materials Science and Applications.* Vol. 3, No. 2, 2014, pp. 58-69.
doi: 10.11648/j.ijmsa.20140302.18

Abstract: In this study, an experimental investigation of thin-walled GMA welded plates of AA5083-H116 has been carried out. The aim of this investigation is to study the effects of the GMAW process on the transient thermal and mechanical phenomena of the welded elements. Thick (4mm) plates of dimensions 700x300 mm^2 were welded using a robotic arm. Measurements of the thermal strains and distortions were performed from the start of the procedure to the end of the cooling cycle together with measurements of the welding thermal cycles in specific positions. After the welding the weld-induced residual stresses field was revealed using the blind-hole-drilling technique while a metallographic examination in different cross sections in the weld area was carried out. The scope of this article is to provide results of combined transient thermal and mechanical phenomena with regards to microstructure of aluminum welded plates.

Keywords: GMAW, Al Alloy 5083-H116, Transient Thermal Phenomena, Mechanical Phenomena

1. Introduction

The design and the erection of a metallic construction that includes welded components introduce special and specific difficulties. The presence of concentrated heat source, basically demanded for the welding of the metallic parts, using arc welding techniques, resulted into adverse effects such as metallurgical changes, residual stresses and deformations in the area of the welding seams [1-4]. Concerning aluminum alloys, its characteristic physical and mechanical properties, such as the relatively high thermal and electrical conductivity, the great solubility of hydrogen in molten aluminum, the elastic modulus and the coefficient of thermal expansion, the latter of which are about the one-third and twice respectively, as much that of steel, exert an adverse influence on the final welded construction [5, 6].

Welding of aluminum alloys has been a subject of numerous studies for many decades. Some of them are devoted to the determination of the strength of the weld [7-9], others focusing on the distribution of the residual stresses near the weld [10, 11] and others on the metallurgical characterization of autogenous and heterogeneous welds [8, 12-15].

The highly localized, non-uniform, transient heating and subsequent cooling of the welded material, occurring during welding, makes the computation and control of the welding thermal cycles a critical first step in predicting imperfections such as high residual stresses, deformations and undesirable microstructural changes. Understanding of the thermal cycles is essential since the temperature has a first order effect on the formation of defects in welds while they have at most a second order effect on the temperature fields [16]. Prediction of the transient and residual stress fields during and after the completion of the welding process, is as a second step to be taken of highly importance, in order to ensure the structural integrity of welded structures. Due to heating and cooling, thermal stresses occur in the weld and the adjacent areas. The strains produced during the heating phase always induce plastic deformation of the metal. The stresses resulting from these strains combine and react to produce internal forces that cause a variety of welding distortions. Welding induced residual stresses and shape-change behavior can play a very important role in the reliable design of the welded joints and welded structures [1, 2, 4, 17].

Though Finite Element Analysis (FEA) has been an effective tool for accurate capturing of thermo-mechanical behavior in welded structures and is being used in the prediction of microstructure, residual stresses and distortion,

for more than two decades [18-23] yet, experimental studies specially focusing in the weld induced residual stresses can be found [24-27].

This research aims at investigating the transient and permanent phenomena following the welding of AA5083-H116 through a series of well controlled experimental techniques. Thus, an in depth experimental investigation of thin-walled GMA welded plates of AA5083-H116 has been carried out. 4mm thick plates of dimensions 700x300 mm^2 were welded using a robotic arm. Measurements of the thermal strains and distortions were performed from the start of the procedure to the end of the cooling cycle together with measurements of the welding thermal cycles in specific positions. After the welding procedure, the weld-induced residual stresses field was revealed by using the blind-hole-drilling technique [28], while a metallographic examination in different cross sections in the weld area was also performed.

Table 1. *Chemical composition of the base metal and filler alloy used (% wt.).*

	Si	Fe	Cu	Mn	Mg	Cr	Zn	Ti
Base Metal: AA5083-H116	0.344	0.224	0.078	0.622	4.573	0.097	0.112	0.014
Filler Metal: AA5356	0.25	0.40	1.10	0.05-0.20	4.5-5.5	0.05-0.20	0.10	0.06-0.20

Table 2. *Mechanical properties of the AA5083-H116.*

Ultimate Strength (MPa)	Yield Strength (MPa)	Modulus of Elasticity (GPa)	Poisson's Ratio	Elongation %
312	241	70.3	0.33	10-12

Table 3. *Welding conditions applied in GMAW.*

Welding Voltage (V)	Welding current (A)	Welding travel speed (cm/min)	Shielding gas flow rate (lit/min)	Shielding gas pressure (bar)	Number of passes
24	160	65	20	5.2	1

2. Experimental Procedure

2.1. Materials and Welding Procedure

The chemical composition of the base metal and filler alloy, AA5083-H116 and AA5356 respectively, can be seen in Table 1 [29] while, the mechanical properties of the AA5083-H116 are presented in Table 2 [30]. Thin plates of dimensions 700x300x4 mm^3 were welded using the welding parameters shown in Table 3.

The filler metal's wire diameter was 1.2 mm, while closed square edge (without any gap) was chosen as edge preparation. Butt welding in flat position was performed by using the robotic arm HITACHI M 6100. Pure Argon was used as a shielding gas.

During welding a ceramic backing strip was attached at the bottom of the position of the specimens to be welded in order to obtain a sound weld profile. In addition, one plate was fully restrained and the other was free from constrains (Fig. 1).

2.2. Transient Phenomena Measurements

Temperature, microstrain and vertical displacement (caused by angular distortion) measurements, were realized during welding and upon cooling in order to monitor the thermal and mechanical response of the welded system. For this purpose, bi-axial surface strain gauges (SG) combined with thermocouples (T) and linear variable displacement transducers (LVDTs) were used during the experimental procedure in order to capture the thermal and mechanical response of the weldments, focusing on the maximum temperatures and cooling rates experienced in the heat affected zone and on the residual angular, out-of-plane, distortion primary at the mid-length of the plates. The location of the sensors is shown in Fig. 1. Regarding SGs, it is mentioned that they were installed both on the face and root surface, at certain and equal positions perpendicular to the weld axis in the mid length of the specimens. This installation enables the measurement of plane and bending micro-strains at the SGs points. During the welding process, the thermal cycles were measured using type-K thermocouples. The thermocouples were positioned in the mid-length and on the top surface of the plates at various distances from the weld line, as shown in Fig. 1. In addition to the thermocouples, (LVDTs) were positioned on the unconstrained surface of the aluminum plate (Fig. 1) in order to measure the vertical deformation, in different locations, during welding and upon cooling. Thermocouples, SGs and LVDTs were all connected to a series of PC-based data acquisition multichannel system (type HBM-SPIDER8), which recorded and processed the measurements using appropriate software.

2.3. Residual Stresses Measurements

The residual stresses at the weld area were later measured using standard rosette strain gauges, suitable for the blind hole-drilling technique (HD). Strain gauge rosettes were positioned on the top surface of the plate (Fig. 1 and Fig. 2) and the blind-hole-drilling technique [31, 32] was employed. The principle of this method is based on the measurement of the relieved strain after the drilling of a small blind hole in the center of the three-element rosette. The measured strain is converted to relieved stress through appropriate equations [32]. The relieved stress is considered to be equal to the residual stress resulting from welding. The technique is applicable to isotropic

linear-elastic materials only.

2.4. Microstructural Characterization

Cross sections of the weld area were cut by mechanical means, properly prepared for metallographic examination by standard procedures and then etched by a Keller's and Barcker`s reagent. Subsequently, samples were examined macroscopically using an optical stereoscope, while microscopic observations were carried out by employing both optical and scanning electron microscopy. Mean values for the grain size of the matrix material exported from the aforementioned micrographs using IMAGE PRO PLUS ANALYSIS image analysis program (according to ASTM E112-10 [33]). Microhardness measurements were performed on cross sections, using a Vickers hardness tester utilizing a 300 g load for 15 s.

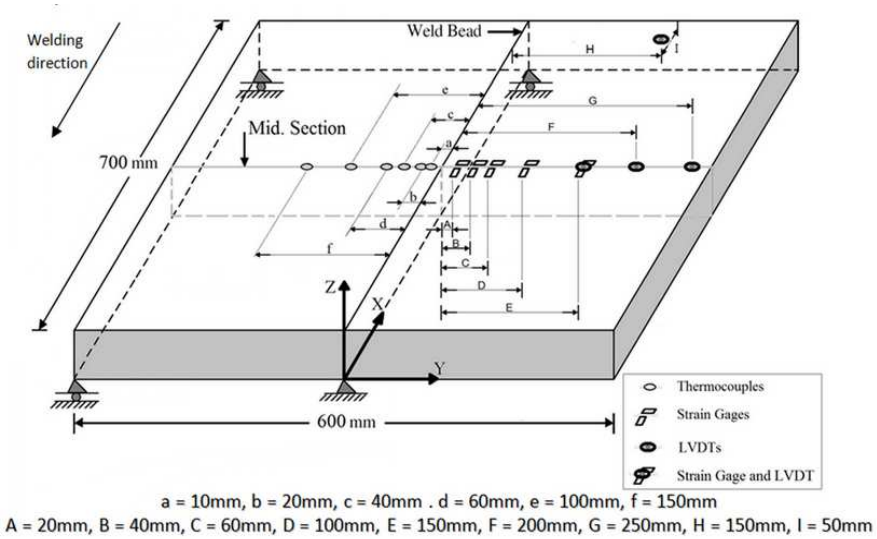

(a)

(b) (c)

Figure 1. a) *Schema of the experimental setup – location of linear variable displacement transducers (LVDT), bi–axial strain gauges (SG) and thermocouples (T), b) strain gauges, c) thermocouples and LVDTs on the top of the plate*

3. Results and Discussion

3.1. Macroscopic Observations

Fig. 3 shows representative macrograph of the cross section of the weldment. As it is shown, the weldment presented sufficient penetration with the fusion zone being clearly vissible. Weld nugget exhibited symmetry in regards to the geometric characteristics, with an average height and width of nugget in the mid-thickness in the order of 6.5 mm and 4.5 mm respectively, and width of root in the order of 4.5 mm (Table 4). Porosity remained in low levels (0.5-0.8%); while no hot cracking phenomena were observed macroscopically.

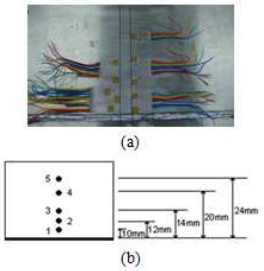

(a)

(b)

Figure 2. a) *Strain gauge rosettes on the top surface of the welded plate, b) positions of strain gauges with regards to the welding axis.*

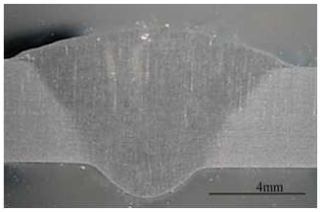

Figure 3. *Macroscopic view of welding zones.*

3.2. Microstructural Characteristics

Microscopic observations in the base metal (BM) revealed that microstructure consisted of elongated grains as a result of cold-working process (Fig. 4a and 4b). EDS analysis results on the large dark particles existing in the Al matrix (Fig. 4a, 4c and 4e) and according to literature [12, 15] lead to the conclusion that correspond to β- phase intermetallic precipitates like Mg_2Al_3 and/or Mg_2Si, along with Al-Mg and Al-Mg-Si. Furthermore, as indicated by EDS analysis results and literature, smaller precipitates (grey particles) correspond to Al-Mg-Fe-Mn phases, like $Al_{12}(FeMn)_3Si$ or $Al_6(MnFe)$ (Fig. 4a, 4d and 4f) [12, 15]. The average grain width was found to be 20-30 μm, while grain length was found to be between 50 μm to 90-100 μm (Fig. 4b).

Table 4. *Geometric characteristics of welding zone.*

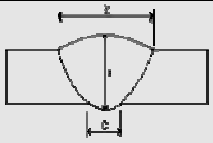

Dimensions of welding zones (mm)		
a	b	c
6.5	8.5	4.5

Heat affected zone (HAZ), exhibited the characteristic microstructure of 5xxx series aluminum alloy weldments that have been subjected to cold working, with emergence of recrystallization, the rate of which is increasing as we approach the weld metal (WM) (Fig. 5a to e).

Near the fusion zone (FZ), HAZ consisted of fully recrystallized and almost equiaxed grains (Fig. 5e) with an average grain diameter of 30 μm (according to ASTM 7.5G).

Regarding the microstructure and grain morphology of WM, it appears that they do not differentiate significantly from those encountered by literature. More precisely, WM near the HAZ (within FZ – see Fig. 3b) presented columnar morphology consisted of elongated cellular dendritic grain growth (Fig. 6a and 6b), with an average width and length, 90 μm and 350 μm, respectively. Also, in the FZ the epitaxial phenomenon is observed, as the initial crystals of WM in the limits of the FZ constitute an extension of the HAZ. In Fig. 6c and Fig. 6d, the appearance of dark areas indicated the formation of interdendritic phases, mainly Mg_3Al_2 [15].

In the center of the WM (Fig. 7), grains appeared to be larger and equiaxed. The average diameter was calculated to be 160 μm (grain size by ASTM: 2.8 G). Furthermore, a uniform distribution of precipitates appeared (Fig. 7c and 7d).

No microcracks were observed in either region of welding area, while weld metal was found to be almost free of micro pores (0.1-0.2%).

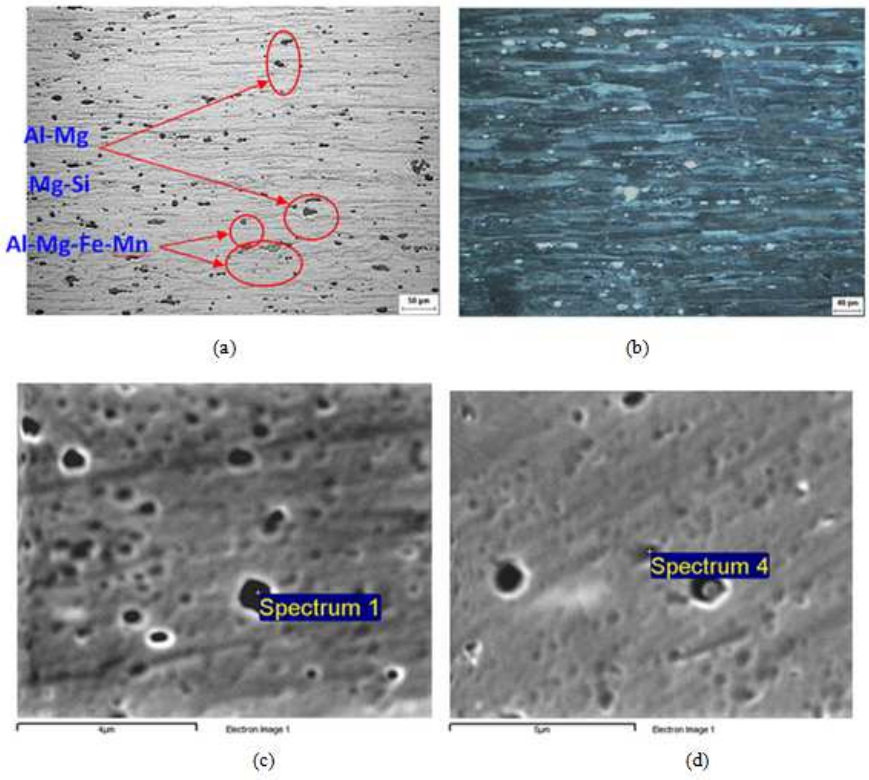

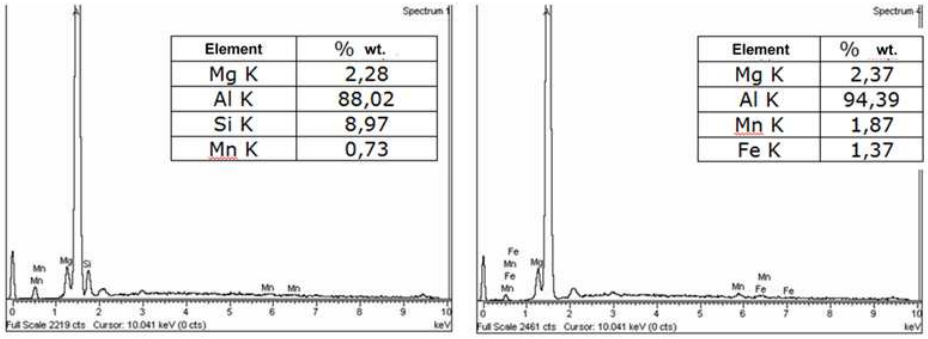

(e) (f)

Figure 4. *Base metal. a) Optical micrograph x200; b) Optical micrograph with polarized light x200;c), d) Scanning electron micrographs, e), f) EDS analysis of spectrum 1 and 4, respectively.*

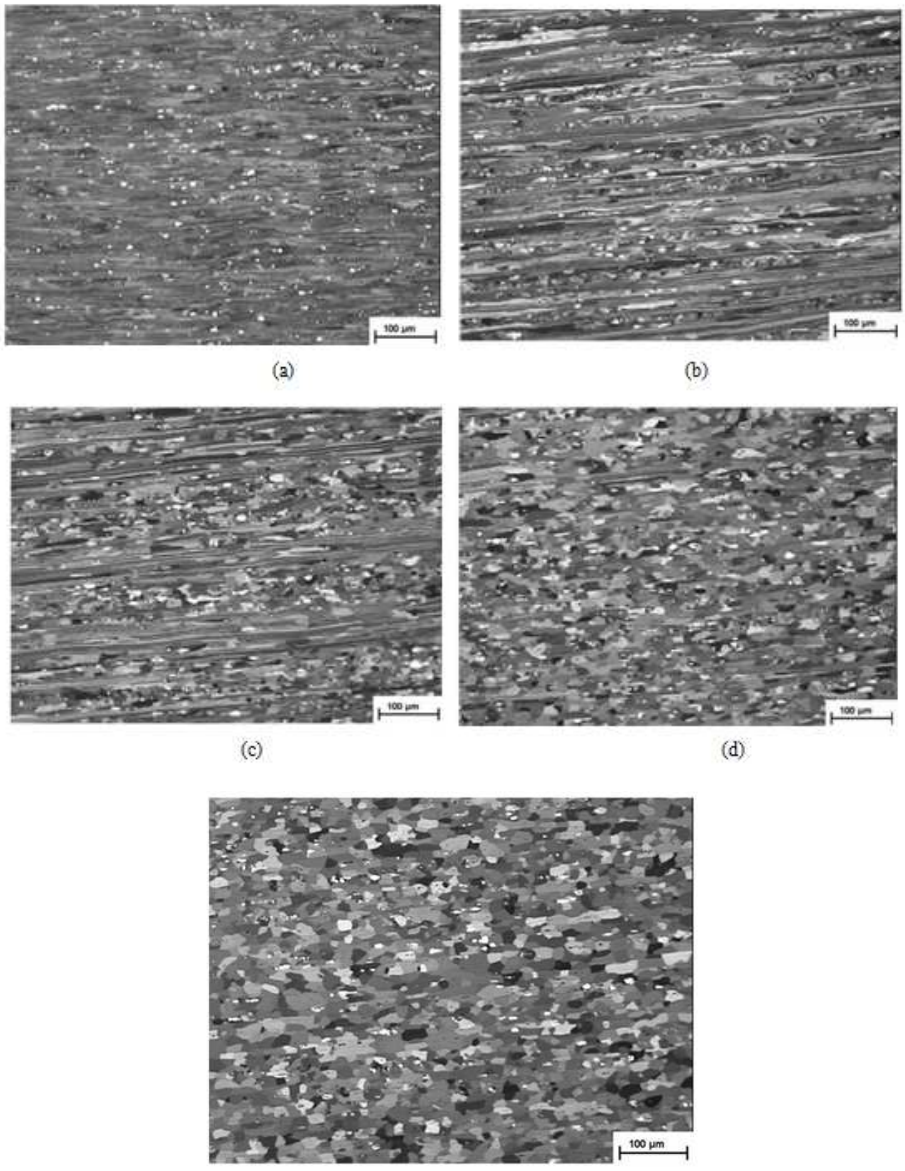

(a) (b)

(c) (d)

(e)

Figure 5. *Optical micrographs of HAZ. Gradually increase rate of recrystallization as we approach the WM (from a to e with a step of 500μm).*

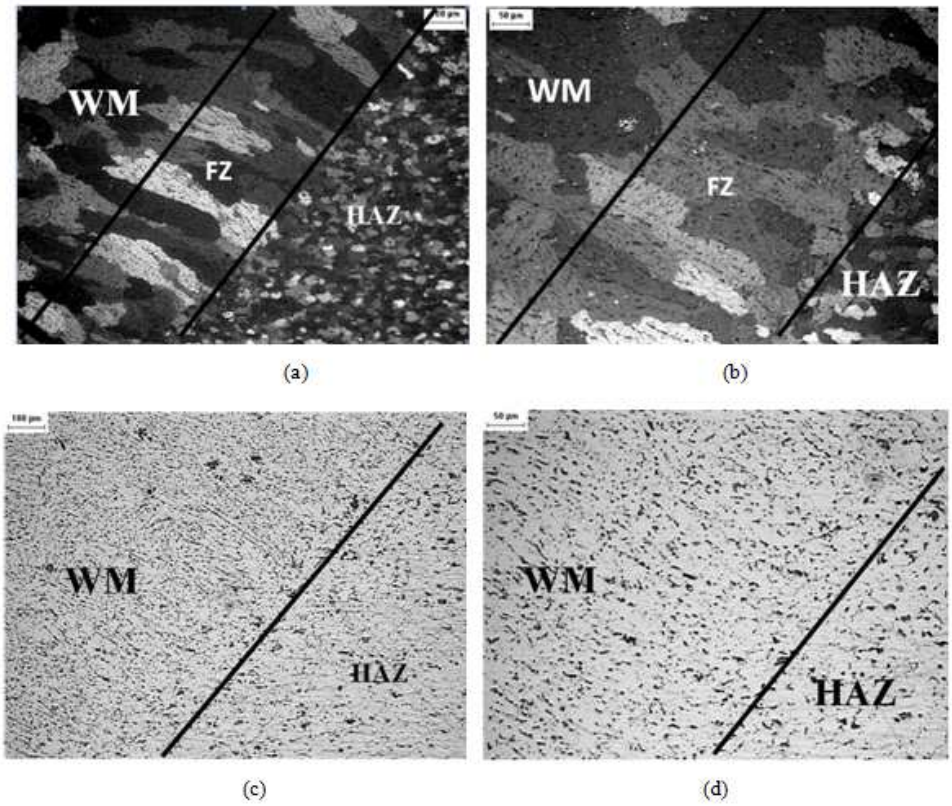

Figure 6. *Optical micrographs of the fusion zone: a) Polarized light b) magnification of a, c) without polarized light d) magnification of c.*

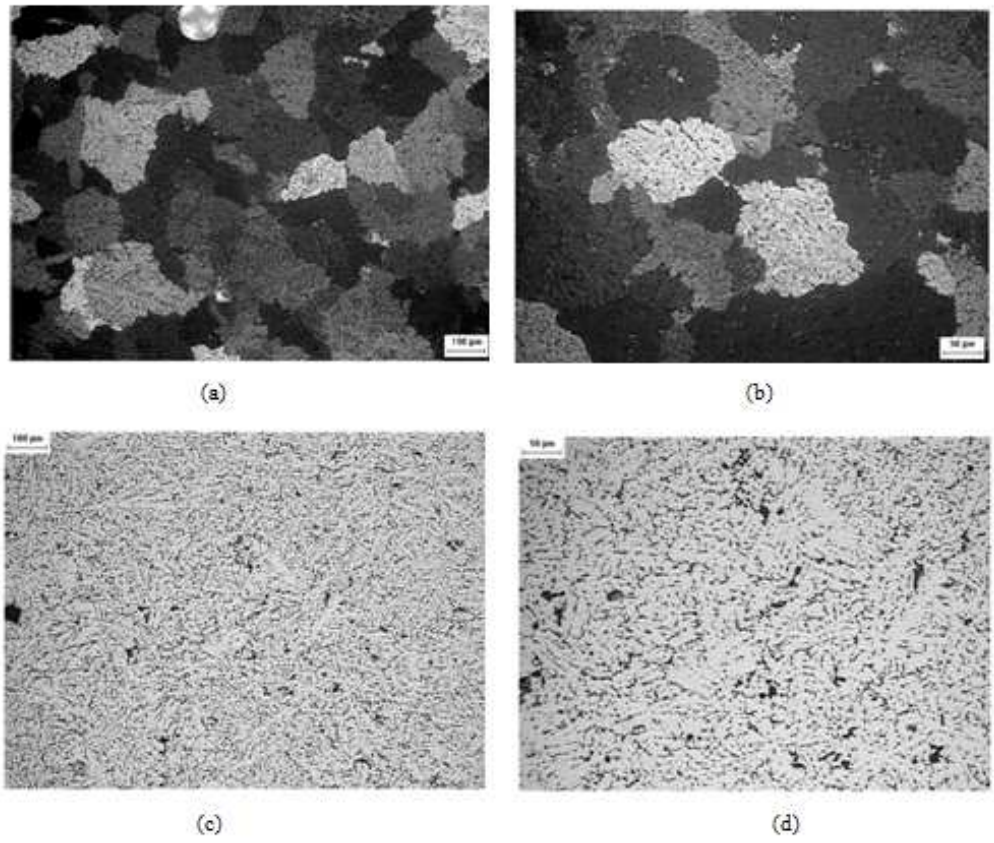

Figure 7. *Optical micrographs of WM. a) Polarized light b) magnification of a, c) without polarized light d) magnification of c.*

3.3. Microhardness Measurements

Microhardness measurements were performed in the mid-thickness and each measurement abstained from the previous a distance of 500 μm.

A gradual decrease, in the order of 20% of microhardness values was observed, from the base metal to the HAZ reaching the value of 80 $HV_{0.3}$ (Fig. 8a) due to graduate recrystallization, and a further slight decrease to the WM in the order of ~75 HV0.3, due to grain morphology (Fig.7).

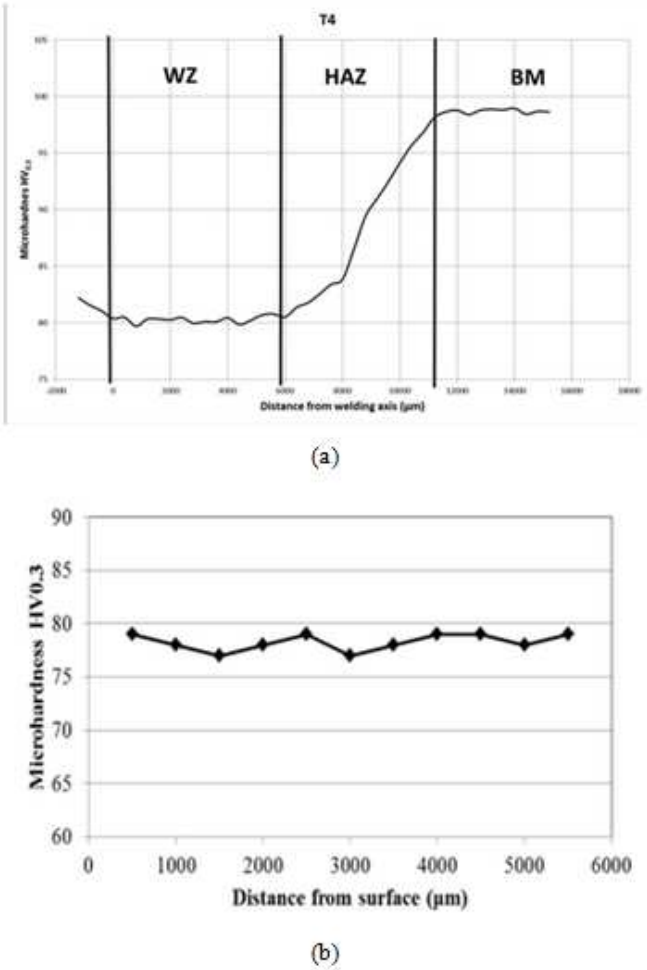

Figure 8. *Microhardness values a) as a function of distance from welding axis, b) as a function of depth in the center of welding zone.*

Furthermore, as presented in Fig. 8b the microhardness profile in the center of the WM, as a function of depth, was kept constant. From the microstructural and microhardness analysis it is evident that though the welding edge preparation adopted promotes great dilution however, the microhardness values in the WM remained in the order of the minimum measured in HAZ (despite the grain growth – Fig. 7a and 7b) revealing the role of the increased percentage in Mg of the filler alloy (Table 1).

3.4. Transient Thermal Cycles

As the measurements of thermal cycles combined with simultaneous measurements of angular distortion during the welding procedure, in the mid-length and width of the specimen, 6 thermocouples were placed as shown in Fig. 1 in order to record the temperature. Fig. 9 presents the measurements of the six thermocouples as a function of time.

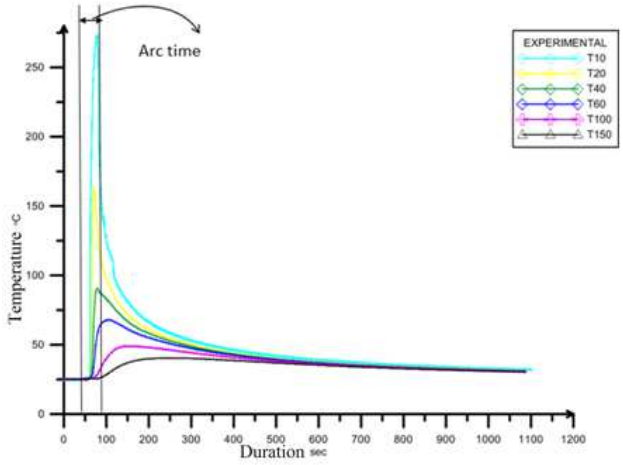

Figure 9. *Transient thermal cycles during welding procedure: T10 – T150 thermocouples at specific distance from welding axis 10mm, 20mm, 40mm, 60mm, 100mm and 150mm, respectively (see also Fig. 1).*

Due to high thermal conductivity of the aluminum alloy in combination with the large dimensions of the specimens, thermocouples gave differences in the obtained maximum values. Especially, in case of first and second thermocouple, the obtained maximum temperatures were 270°C and 170°C, respectively; giving thus abrupt temperature changes for areas near the welding seam and more smooth in regions away from it. Furthermore, great temperature differences between thermocouples were expected as a result of thermal properties of aluminum alloy, indicating the existence of residual stresses, distortions and deformations. Hence, in a distance of 40 mm from the welding axis (thermocouple T40), temperature reached the maximum value of 90°C, while, as can be seen from the temperature profiles given by all thermocouples, in less than 80 s from the end of the welding procedure, specimen acquires temperatures of less than 100°C. In addition, in a distance of 10mm from the welding axis (thermocouple T10) temperature did not exceed 270°C, leading to the conclusion that recrystallization of the material has not occurred. This comes to an agreement with microhardness values as one can observe in Fig. 8a.

3.5. Transient Thermal Stress, Distortion, Deformation and Residual Stresses

3.5.1. Vertical Displacement Curves as a Function of Time

By analyzing curves in Fig. 10, combined with the

experimental setup of Fig. 1, it can be concluded that after the start of the welding procedure, vertical displacements due to angular distortion took negative values (negative axis is defined as the axis towards the root of weld) as a result of heating and melting of the welding edges which led to metal expansion. Vertical displacement caused by angular distortion obtained its maximum negative value (in the order of 2 mm) by the time the arc passes the transverse axis (relative to the welding axis), at 32 sec (middle length of the plate), in which LVDTs are installed (Fig. 1a). As the arc moved away of this region, welding metal started to solidify and cooling procedure started followed by its contraction. Consequently, the vertical displacement caused by angular distortion gradually begins to increase, acquiring positive values (positive axis is defined as the axis with direction to the welding gun) and finally at the end of the cooling cycle, after approximately 1000 sec from the beginning of the welding procedure, the maximum vertical displacement was recorded in the order of 8.25 mm.

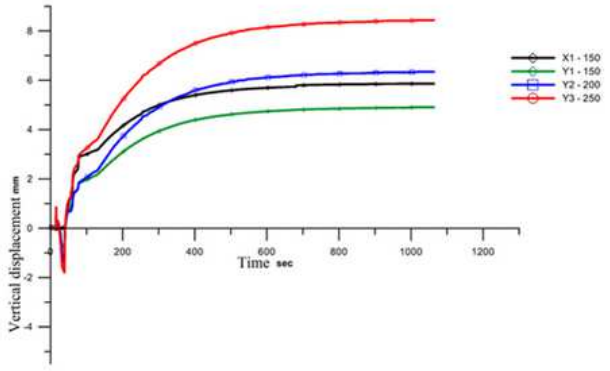

Figure 10. *Vertical displacement curves as a function of time (X1-150 is the LVDT located at a distance of 150mm from weld axis close to the welding start, while Y1-150, Y2-200 and Y3-250 are LVDTs located at the mid length of the welded plates, at distances of 150mm, 200mm and 250mm from the weld axis, respectively. See also Fig. 1).*

It is noticeable that although LVDTs X1-150 and Y1-150 were in the same longitudinal axis, parallel to weld axis and expected to give the same vertical displacement caused by angular distortion values, nevertheless, they presented a difference in the order of 1 mm, due to longitudinal bending distortion and buckling distortion.

3.5.2. Transient Strains Curve as a Function of Time

Thermal deformation during welding is the result of complex mechanisms including among others plastic deformation which takes place in a wide temperature range, from room temperature to the melting point of the metal. As welding procedure is envolving, temperature distribution continuously alters, causing alterations in contraction and deformation of welded specimens. From the weld start and as the torch approaches the region where strain gauges are installed the material is gradually heated and expansion occurs due to temperature increase, indicating the development of compressive stresses, as the expansion is constrained by neighbor lower temperature areas. Immediately after the arc passes the axis where strain gauges are installed, cooling of materials is starting and thus its contraction. In this case, tensile stresses are developing as the contraction is constrained by neighbor higher temperature areas. As the plate continues to cool down, behind the arc and after welding completion, temperature decreases in low levels, deformation stops to evolve and equilibrium has occurred. From Fig. 11a referring to the transient micro-strains in direction parallel to the weld line (X-direction), in different distances from the weld axis (20 mm, 40 mm, 60 mm, 100 mm and 150 mm respectively), on face surface (U-surface), it can be seen that closer to the weld zone and at distance in the order of 40 mm the residual micro-strain, after cooling, was negative indicating contraction and thus tensile stresses. At distances greater than 40 mm the residual micro-strain had low positive value indicating low expansion thus low compressive stresses. Concerning Fig. 11b referring to the transient micro-strains in direction parallel to the weld line (X-direction), in the same distances from the weld axis, on root surface (D-surface), residual micro-strain had in any case negative value indicating contraction and thus tensile stresses. The difference in response between the face and the root surface was because of the longitudinal bending distortion and possible local buckling distortion.

Having the advantage of the measurements on both surfaces of the plate at the same point, by taking the mean value of the microstrains measured, the plane-microstrains can be revealed (Fig. 11c) while by taking the semi-difference of the microstrains measured, bending-microstrains can be revealed (Fig. 11d). Again, concerning plane-microstrains (Fig. 11c), closer to the weld zone and at distance in the order of 40 mm the residual plane-microstrain, after cooling, was negative indicating contraction and thus tensile stresses while at distances greater than 40 mm the residual plane-microstrain had low positive value indicating low expansion thus low compressive stresses. Concerning the residual bending-microstrains (Fig. 11d) only at distance 20 mm from the weld line recorded a negative value while other values were positive.

From Figs. 11a to 11d it was evident that values of microstrains recorded at the distance of 20 mm from and at direction parallel to the weld axis, had significant value, compared to the values at other distances, suggesting the formation of significant tensile (negative value in any case) residual stresses up to this distance.

From Fig. 12a referring to the transient microstrains in direction perpendicular to the weld line (Y-direction), in different distances from the weld axis (20 mm, 40 mm, 60 mm 100 mm and 150 mm respectively), on face surface (U-surface), it can be seen that closer to the weld zone and at distance in the order of 20 mm the residual microstrain, after cooling, was positive, indicating expansion and thus compression stresses. At distances greater than 20 mm the residual microstrain had low negative values indicating low

contraction thus low tensile stresses. Concerning Fig. 12b referring to the transient microstrains in direction perpendicular to the weld line (Y-direction), in the same distances from the weld axis, on root surface (D-surface), residual microstrains had in any case low negative values indicating contraction and thus tensile stresses. The difference in response between the face and the root surface was because of the longitudinal bending distortion and possible local buckling distortion.

Again the plane-microstrains (Fig. 12c) and the bending-microstrains (Fig. 12d) were revealed by taking the mean values and semi-differences of the microstrains recorded respectively. Concerning plane-microstrains in Y-direction (Fig. 12c), closer to the weld zone and at distance in the order of 20 mm the residual plane-microstrain, after cooling, is positive indicating expansion and thus compressive stresses while at distances greater than 20 mm the residual plane-microstrains had low negative values indicating low contraction thus low tensile stresses. Concerning bending-microstrains (Fig. 12d) the values recorded were in any case negative.

From Figs. 12a to 12d it was evident that values of microstrains recorded at the distance of 20 mm from and at direction parallel to the weld axis, had significant value, compared to the values at other distances, suggesting the formation of tensile (negative value in any case) residual stresses up to this distance which however were significantly lower than the corresponding value to the X-direction (300 με to 1200 με respectively).

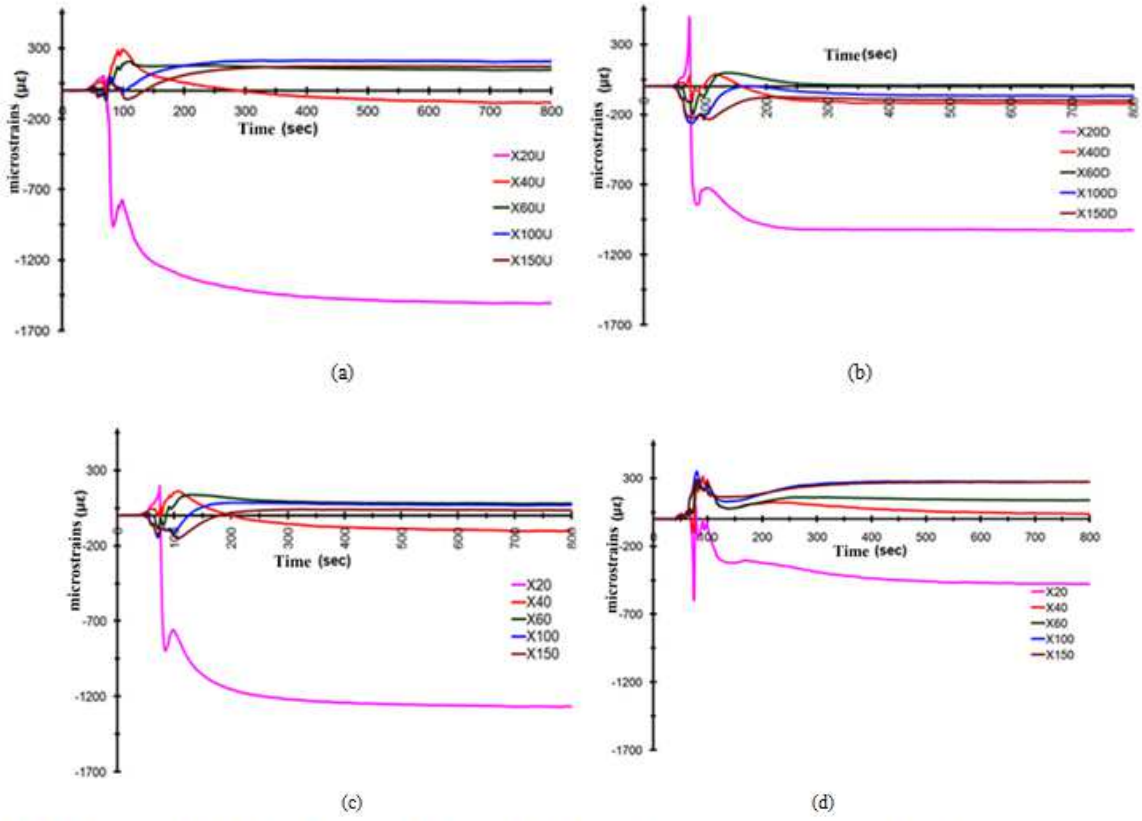

Figure 11. Transient strains curve as a function of time a) micro-strains x- axis upper surface (U), b) micro-strains x- axis root surface (D), c) the plane-micro-strains x-axis (P) and d) bending-micro-strains x-axis (B).

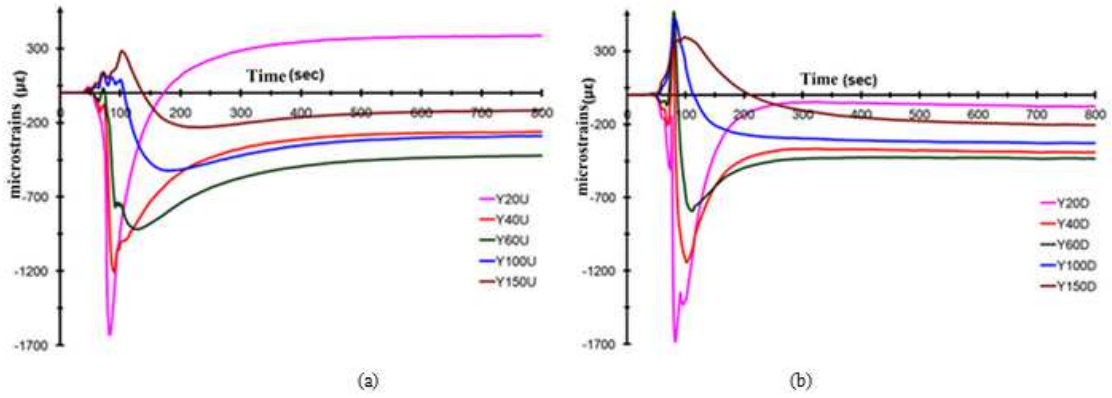

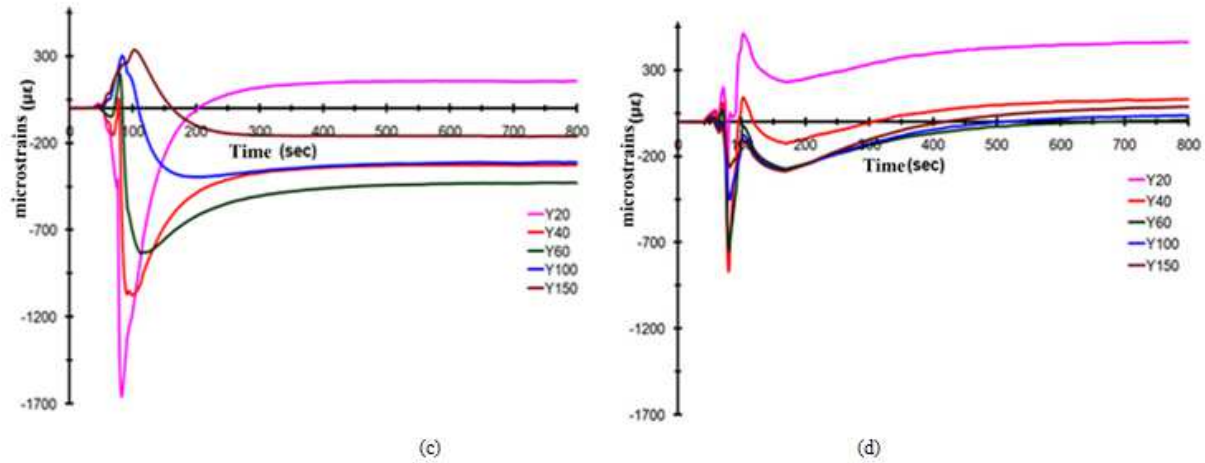

Figure 12. *Transient strains curve as a function of time a) micro-strains y- axis upper surface (U), b) micro-strains y- axis root surface (D), c) the plane-micro-strains y-axis and d) bending-micro-strains y-axis.*

3.5.3. Residual Stresses

Fig. 2 shows the arrangement of strain gauges on the top surface of the welding specimen. As the method restrictions impose the distance between the two measurements to be greater than the size of a rosette (~10 mm) in order to take interim measurements, two rows of rosettes were mounted in the axis transverse to the welding axis. All measurements were performed on the top surface of the plates, with the first measurement taken at a distance of about 15mm from the welding axis.

Fig. 13 shows the results of residual stresses measurements by blind-hole-drilling technique as a function of distance from the weld axis. In the zero distance of the welding axis residual stresses are tensile in the order of yield stress of the material at room temperature (≈240 MPa).

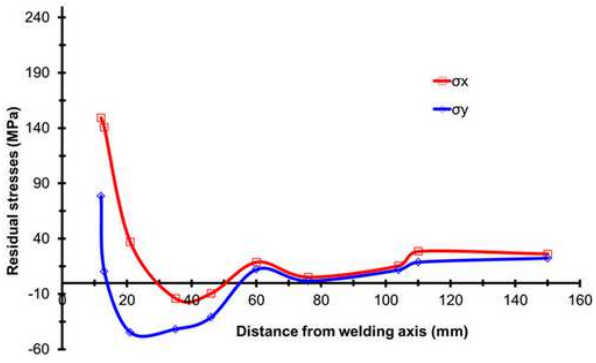

Figure 13. *Residual stresses measurements by hole drilling technique.*

From Fig. 13, it can be concluded that the longitudinal residual stresses (σx) were tensile and constantly decreased as the distance from the welding axis was increased and up to 30 mm in distance from it. In 15 mm distance from the welding axis, where the first measurement was taken, the longitudinal residual stress (σx) had the maximum value in the order of 169 MPa. After the distance of 30 mm from the welding axis, residual stresses became compressive; taking however small values, and then at a distance of 55 mm turned into tensile due to the longitudinal deflection of the welded plate. The transverse residual stresses (σy) showed the same pattern with more restricted zone of tensile stresses and wider of the compressive ones. Residual stresses patterns and values correspond to measurements found in literature [16].

4. Conclusions

Based on the aforementioned results, several conclusions can be drawn:

- A sufficient penetration was achieved with the weld nugget exhibiting symmetry in regards to its geometric characteristics. Defects like porosity or hot cracking was not observed.
- As far as microstructure is concerned, the rate of recrystallization increased while moving from the BM to the FL. In the region of the HAZ close to the FZ, fully recrystallized, almost equiaxed grains were observed. Segregation was revealed in the FZ with the grain morphology changing from columnar (close to the fusion line) to large equiaxed in the center of the WM.
- Microhardness measurements followed the evidences of the microstructure characterization showing a gradual decrease of values from the base to the weld metal all through the HAZ. The role of the increased percentage in Mg of the filler alloy was revealed as the microhardness values didn't drop any further, in the center of the WM, from the minimum values in the HAZ despite the large equiaxed grains of that area.
- Recrystallization temperature occurred at distance from the weld axis less than 10 mm since the maximum temperature measured at 10 mm was 270oC. At distances greater than 10 mm, the maximum temperature observed was not likely to cause any change in the microstructure of the material. The profile of the thermal cycles was in agreement with the microstructure and microhardness analysis.

- Vertical displacement due to angular distortion changed from negative (as the welding procedure was developing) to positive values (after the completion of the procedure), due to high thermal conductivity, expansion and contraction of the material. The maximum negative value (in the order of 2 mm) was reached at the moment the arc passes the transverse axis (middle length of the plate) while, the maximum positive value (in the order of 8.25 mm) was recorded more than 900 sec from the completion of the welding procedure. It is worth to be noticed that vertical displacement acquired "zero" value at the completion of the welding procedure (~64 sec).
- From the weld start and as the torch approaches the region where strain gauges were installed the material is gradually heated and expansion occurs due to temperature increase, indicating the development of compressive stresses, as the expansion is constrained by neighbor lower temperature areas. Immediately after the arc passes the axis where extensometers were installed, cooling of materials is starting and thus its contraction. In this case, tensile stresses are developing as the contraction is constrained by neighbor higher temperature areas. As the plate continues to cool down, behind the arc and after welding completion, temperature decreases in low levels, deformation stops to evolve and equilibrium was occurred.
- Results obtained by residual stresses measurements found to be in agreement to the profile of final values of transient strains curves as a function of time. More specifically, at a distance of 20 mm from welding axis, significant values of tensile residual stresses were measured, while as can be seen from Fig. 11, X20U, X20D, X20P and X20B final values have significant difference as compared to the values measured at greater distances.

References

[1] Masubuchi, K. "Analysis of Welded Structures". Oxford Pergamon Press, 1980.

[2] Radaj, D. "Heat Effect of Welding: Temperature Fields, Residual Stress Distortion". Berlin Springer, 1992.

[3] Mathers, G. "The Welding of Aluminum and its Alloys". Cambridge (England), CRC Press, 2002.

[4] Puchaicela, J. "Control of Distortion of Welded Steel Structures", Welding Journal, Vol. 77, 1998, pp. 49–52.

[5] Martukanitz, R. "Selection of Nonferrous Low Temperature Materials". In ASM Metals Handbook, Vol. 6, Welding, Brazing and Soldering, American Society of Materials International, Materials Park, OH, USA, 1993.

[6] Dickerson, P. "Welding of Aluminum Alloys". In: ASM Metals Handbook, Vol. 6, Welding, Brazing and Soldering, American Society of Materials International, Materials Park, OH, USA, 1993.

[7] Goldak, J. A., Chakravarti, A., Bibby, M. "A New Finite Element Model for Welding Heat Source". Metallurgical Transactions B, Vol. 15, No. 2, 1984, pp. 299-305. doi:10.1007/BF02667333.

[8] Kamala, V., Goldak, J. A. "Error Due to Two Dimensional Approximations in Heat Transfer Analysis of Welds". A.W.S. Welding Research Supplement, Vol. 76, No. 9, 1993, pp. 440s–446s.

[9] Tsai, C.L., Park, S.C., Cheng, W.T. "Welding Distortion of a Thin-Plate Panel Structure". A.W.S. Welding Journal, Research Supplement, Vol. 78, 1999, pp. 156s–165s.

[10] Lindgren, L.E. "Numerical modeling of welding". Computer Methods in Applied Mechanics & Engineering, 195 (2006), 6710–6736.

[11] Deng, D., Murakawa, H., Liang, W. "Numerical simulation of welding distortion in large structures". Computer Methods in Applied Mechanics & Engineering, 196 (2007), 4613–4627.

[12] Deng, D., Murakawa, H. "Numerical simulation of temperature field and residual stress in multi-pass welds in stainless steel pipe and comparison with experimental measurements", Computational Materials Science, 37 (2006), 269–277.

[13] Gannon, L., Liu, Y., Pegg, N., Smith, M. "Effect of welding sequence on residual stress and distortion in flat-bar stiffened plates". Marine Structures 23 (2010), 385–404.

[14] Attarha, M.J., Sattari-Far, I. "Study on welding temperature distribution in thin welded plates through experimental measurements and finite element simulation". Journal of Materials Processing Technology 211 (2011), 688–694.

[15] Kenno, S.Y., Das, S., Kennedy, J.B., Rogge, R.B., Gharghouri, M. "Residual stress distributions in ship hull specimens". Marine Structures 23 (2010), 263–273.

[16] Silva, C.C., Farias, J.P. "Non-uniformity of residual stress profiles in butt-welded pipes in manual arc welding". Journal of Materials Processing Technology 199 (2008), 452–455.

[17] Pearce, S.V., Linton, V.M., Oliver, E.C. "Residual stress in a thick section high strength T-butt weld". Materials Science and Engineering A 480 (2008), 411–418.

[18] Lee, C.-H., Chang, K.-H. "Temperature fields and residual stress distributions in dissimilar steel butt welds between carbon and stainless steels". Applied Thermal Engineering 45-46 (2012), 33-41.

[19] Sonsino, C.M., Radaj, D., Brandt, U., Lehrke, H.P. "Fatigue assessment of welded joints in AlMg4.5Mn aluminum alloy (AA 5083) by local approaches" International Journal of Fatigue, Vol.21 (1999), 985–999.

[20] Chan, T.K., Porter Goff, R.F.D. "Welded aluminum alloy connections: test results and BS8118" Thin-Walled Structures, Vol.36 (2000), 265–287.

[21] Calcraft, R.C., Wahab, M.A., Viano, D.M., Schumann, G.O., Phillips, R.H., Ahmed, N.U. "The development of the welding procedures and fatigue of butt-welded structures of aluminium-AA5383". Journal of Materials Processing Technology Vol.92-93 (1999), 60-65.

[22] Canas, J., Picon, R., Paris, F., Blazquez, A., Marin, J. C. "A simplified numerical analysis of residual stresses in aluminum welded plates" Computers & Structures, Vol. 58 No. 1 (1996), 59-69.

[23] Luh, G. C. and Hwang, R. M. “Measuring Non-Uniform Residual Stress in Thin Plates by a Proposed Hole-Drilling Strain Gauge Method”. International Journal of Advanced Manufacturing Technology, Vol. 15 (1999), 103–113.

[24] Menzemer, C., Lam, P.C., Srivatsan, T.S., Wittel, C.F. “An investigation of fusion zone microstructures of welded aluminum alloy joints”. Materials Letters, Vol.41 (1999), 192–197.

[25] Katoh, S. “Pulsed TIG welding of aluminium”. Welding International, Vol.4, No. 12 (1990), 944-953.

[26] Luijendijk, T. “Welding of dissimilar aluminum alloys”. Journal of Materials Processing Technology, Vol.103 (2000), 29-35.

[27] Katsas, S., Nikolaou, J., Papadimitriou, G. “Microstructural changes accompanying repair welding in 5xxx aluminium alloys and their effect on the mechanical properties”. Materials and Design 27(2006), 968–975

[28] American Society for Testing Materials (ASTM). 2001. Designation: E837–Standard test method for determining residual stresses by the hole-drilling strain-gage method. ASTM International.

[29] ASM Handbook, Properties and Selection: Nonferrous Alloys and Special-Purpose Materials, 10th ed., 1990, Vol. 2, ASM.

[30] AWS, ‘Guide for Aluminum Hull Welding’, 1983, D3.7-83, ANSI/AWS

[31] Vishay Group. 1993. Technical notes: TN-503, measurement of residual stresses by the hole-drilling strain gauge method. Measurements Group Inc.

[32] American Society for Testing Materials (ASTM). 2001. Designation: E837–Standard test method for determining residual stresses by the hole-drilling strain-gauge method. ASTM International.

[33] American Society for Testing Materials (ASTM). 2012. Designation: E112-10 Standard Test Methods for Determining Average Grain Size.